

# Trend on Silicon Technologies for Millimetre-Wave Applications up to 220 GHz

Gaëtan Prigent <sup>1</sup>, Thanh Mai Vu <sup>2</sup>, Eric Rius <sup>3</sup>, Robert Plana <sup>2</sup>

<sup>1</sup> *Université de Toulouse; INPT, UPS ; CNRS LAPLACE ; France*

<sup>2</sup> *Université de Toulouse ; UPS, INSA, INPT, ISAE ; CNRS LAAS ; France*

<sup>3</sup> *Université Européenne de Bretagne ; Université de Brest ; CNRS Lab-STICC ; France*

## 1. Introduction

Largely reserved for military applications at the origin, the field of transmissions by electromagnetic waves is strongly prevalent in recent years with the emergence of new applications. Recent evolutions in modern civilian millimetre-wave applications, such as collision-avoidance radar sensor, inter-satellite communications, pico-cell networks, and microwave imaging have led to hardened constraints in terms of selectivity, performances, and bulk reduction. In this frequency range, a high level technological resolution is needed at low wavelength. This means that millimetre-wave monolithic integrated circuits (MWMICs) are generally preferred to hybrid technology.

Moreover, with the constant evolution of systems in millimetre wave frequency range, the ever growing mass market forced the technological to reduce their costs of production. Thereby, technologies usually reserved to millimetre-wave applications, such as III-V technologies (InP or GaAs), have reduced their use for the benefit of silicon clusters. Indeed, III-V technologies have been for a long time the unique ones able to address millimetre-wave applications. One of the major advantages of III-V technologies is their low loss level; nevertheless their cost is prohibitive for general public applications and limited to a small series production. Conversely, silicon technologies which are more economics, present level of losses too high to meet drastic specifications of actual systems, especially for passive functions. Thereby, recently many studies were led to take advantage of silicon technology for the integration of passive functions on active chip. The trend was reversed since Si-based technologies now offer competing performances. Si-based technologies are indeed cheaper, which is reinforced by their high integration capabilities. Then increasing efforts have been carried out during the past years to evaluate the potential of silicon technologies to address millimetre-wave applications. For instance, the 7 GHz unlicensed bandwidth around 60 GHz and 77 GHz for automotive radar applications has focussed many attention since large volumes can be expected for those applications. Due to its cost advantage, improved millimetre-wave transistor characteristics, and ease of integration of high performance digital and high speed analog/RF circuits, silicon has emerged as the favourite solution satisfying the needs of rapidly growing communications market, and is now a competitive

alternative to classical III-V technologies to address millimetre-wave applications. Moreover, next-generation silicon-based RF CMOS and BiCMOS technologies, which offer NMOS and SiGe HBT devices with cutoff frequencies beyond 277 GHz (Kuhn et al., 2004) and 300 GHz (Rieh et al., 2004) respectively, will enable the implementation of millimetre-wave system-on-chip (SoC) such as 60 GHz WLAN (Floyd et al., 2006),(Doan et al., 2004), 40/80/160 Gb/s optic-fiber transceivers (Perndl et al., 2004) or 24/77 GHz collision avoidance radars, which were reserved until recently to III-V compound semiconductors application domain.

However, integration of high performances passive components remains a key issue in silicon technologies. Some of the available solutions consists in the use of silicon as a support for active function development, passive functions being implemented on silicon using specific technologies such as membrane technologies (Vu et al., 2008) or thin film microstrip (TFMS) based technologies developed on Si-BCB substrate (Six et al., 2006), (Prigent et al., 2004), (Wolf et al., 2005). Nevertheless, if such technologies have already proved their efficacy for sub-millimeter wave functions, their implementation remains difficult since they need complex technological process. Recent work (Gianesello et al., 2006) have demonstrated that silicon technologies are able to address higher frequencies applications up to G-band (140-220 GHz) if high resistivity (HR) silicon-on-insulator (SOI) technology is used. Moreover, feasibility of integrated antenna made on advanced CMOS standard technology has been demonstrated (Montusclat et al., 2005) and HR SOI technology has proved its efficacy to improve the overall performances of integrated antennas. However, in millimeter frequency range, the design of narrow-band planar filters appears as one of the most critical point. Hence, in view of the required selectivity levels, designers are, indeed, faced with problems in relation to control design, i.e. modelling accuracy, as well as the high insertion loss levels inherent in such devices. Moreover, due to low electrical lengths involved in millimetre-wave, the technological dispersion has to be as low as possible.

This chapter is aimed at describing the evolution of technological processes for the design of passive functions in millimetre-wave frequency range. III-V technologies that are behind the development of millimetre-microwave functions in W-band are first described. Performances obtained in III-V technology for wide- and narrow-band filters reported here will be the reference for comparison with other technologies. Several technological process dedicated to silicon technologies were then studied: membrane and thin film microstrip technologies. Finally, millimetre-wave electrical performances of devices were reported for passive components and active circuits achieved in ST-Microelectronics advanced CMOS HR SOI technology, so as to investigate the suitability of that technology to address millimetre-wave Systems on Chip (SOC) up to 220 GHz and beyond. Classical stub-based broadband filters implemented in coplanar waveguide technology were first designed so as to prove the technological process accuracy as well as its performances which are fully competitive with III-V technologies. Then, the design of coupled-lines narrowband filters was investigated in the V-band, at 60 GHz. These concepts were validated through comparison with experiments performed up to 220 GHz.

## 2. III-V Technology Application

### 2.1 Technological process

The first technology cluster that we present is the III-V (either GaAs or InP) technological process developed in the IEMN laboratory of Lille, France. The use of semi-conductor substrate allows taking advantage of transport properties of charge inherent in this material for active functions implementation (transistor for instance) (Dambrine et al., 1999). Thus, such a technology offers the possibility to realize millimetre-wave monolithic integrated circuits (MWMICs) for which passive and active components are made on the same medium. Thereby, the losses induced by the surface mounting and the wiring of the components are reduced, as well as the cost of production.

This technology is based on the deposit of successive metal layers. Due to its good conductivity ( $\rho \approx 4.1 \cdot 10^{-7}$ ) as well as its high resistance to oxidation, metal widely used for III-V technologies is gold. In millimetre frequency range, gold thickness is an important parameter, generally 3- $\mu\text{m}$ -thick, so as to reduce propagation losses. Several techniques are possible to achieve this metallic deposit. The usual plating techniques such as vacuum evaporation or spraying are costly when the metal thickness exceeds the micron. That is why, in order to minimize costs, the filing of metallization is by electroplating. We will briefly describe the steps needed to implement components in III-V technology, namely technology of electroplating and lithography combined, as well as the masks topology.

The basic principle of the technology studied hereafter is the deposit of successive layers of sacrificial photoresist layers. The sacrificial layer parts that are subject to insulation are etched and eliminated after dilution onto remover. Therefore, patterns are defined through optical masks used in the phases of the sacrificial layer insulation. In the described technology, two optical masks were used: the first whose dimensions are higher (3  $\mu\text{m}$ ) than the actual pattern dimensions, the second having the exact dimensions. The use of such a process allows, if there is no overlap between the two sacrificial layers, to avoid bulges forming on the edge of the patterns during the metallization. Moreover, this process allows an extra margin for alignment of optical masks, preciseness in alignment being of the order of micron.

So as to perform electroplating, it is necessary to make conductor the pattern to be metallic. So a thin metal layer (few hundred angstroms) is deposited either by vacuum evaporation or by cathode spraying. This last technique is preferred to the first one since it avoids tearing of the sacrificial layers, and therefore the protected patterns. Moreover, it allows a greater rigidity of the metallic layer. In conventional III-V technologies, this thin metal layer is composed of a 200- $\text{\AA}$ -thick titanium layer to ensure a good adhesion followed by a 300- $\text{\AA}$ -thick gold deposit that allows metal growth. Indeed, because of the strong oxidation of titanium in air, it is virtually impossible to achieve electrolysis directly on the titanium.

Once electroplating performed the adhesion layer is chemically etched. Nevertheless, during the etching of the device, both adhesion layer and gold deposit are etched. Moreover, for patterns of low dimensions, it is necessary to insist in the etching process, this has the effect of reducing the metal thickness and size of the pattern, but also to increase the roughness of the deposit. One should also remark that, most of the time, during the etching process, there is a slight film of gold to prevent the titanium etching which creates short-circuits between patterns. For this reasons, the proposed technology uses a nickel deposit that satisfies all the requirements: a good substrate adhesion, a good gold-growth and ease in etching process.

The third step consists in electroplating itself, once achieved patterns definition and thin metal layer deposit phases. An electric current flow in an electrolyte solution (solution of double cyanide of gold and potassium ( $\text{KAu}(\text{CN})_2$ )) creates a chemical reaction near electrodes. Gold ions being positive, the sample foil is attached to the cathode. It follows a phenomenon of transfer of charges called electroplating. This basic principle is relatively simple; however this operation must still be undertaken with some caution. Indeed, ohmic losses of a transmission line depend not only on the resistivity of the metal, but also to its surface state. But the roughness of the metallic layer increases with the current density. It is therefore necessary to apply a current density relatively low. However, if very low current density yields a very low roughness, it also increases the time of filing causing problems of mechanical strength of the sacrificial layer. We must therefore find a compromise between roughness and mechanical strength.

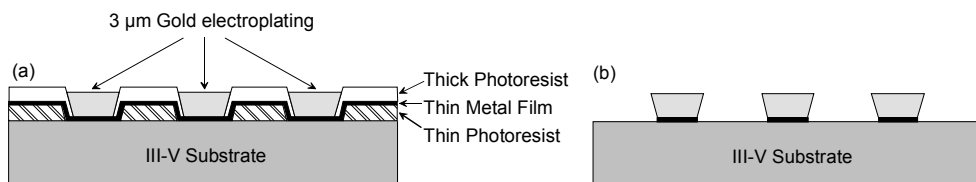


Fig. 1. Transmission line realization: a- Lithography process, b- Transmission lines after sacrificial layer removing and thin metal layer etching.

In the millimetre and sub-millimetre frequency range coplanar waveguides are more commonly used in the design of circuits (Argarwal et al., 1998), (Haydl et al, 1999), (Hirose et al., 1998), (Papapolymerou et al., 1999). Many studies have, indeed, shown that coplanar waveguides can be considered as a good alternative to microstrip lines in this frequency range (Houdard, 1976), (Hirota & Ogawa, 1987), (Ogawa & Minagawa, 1987), (Brauchler et al., 1996), (Kulke & Wolff, 1996), (Herrick et al., 1998). Because all conductors are located on the same plane, the ground connections through via-holes are eliminated and no reverse side processing is needed, which significantly reduces cost. Because of the large decoupling between the different elements of a coplanar system, global size reduction may be obtained as well. Another advantage of the coplanar technology is flexibility in the design of the passive circuits. Indeed, a large number of geometrical parameters can be chosen to design a transmission line with given impedance.

Electrical characteristics can then be improved by correctly defining the ratio between the strip width and the slot width. However, designers are faced with two major drawbacks when they deal with coplanar technology. The first one is the lack of mature equivalent-circuit models like those available for microstrip lines. The second one concerns the suppression of the fundamental, but parasitic, slot line mode that may be excited by non symmetrical coplanar waveguide discontinuities such as, for example, bends or T-junctions. The suppression of such perturbing modes is achieved by inserting bridges over the centre conductor, so that the potentials on either side of the lateral ground planes are identical (Koster et al., 1989), (Beilenhoff et al., 1991). Consequently, additional steps in the production process are needed for the fabrication of the bridges.

There are two types of air-bridges: classical inter-ground and inter-conductor bridges, their role is to force a similar voltage on either side of the central conductor. Whatever the bridge

topology, the technological process for bridge realization is identical and similar to the technological process described above (Fig. 2). Besides the good definition for devices due to the high-resolution technology, one of the advantages of this technological process is the control of the shape of the air-bridge. Indeed in hybrid technology, air-bridges are generally implemented by using wire-bonding connected manually to the ground plane. By such a process the shape of the bridge is difficult to control involving a problem of reproducibility first and in the other hand problems with bridge modelling. Here, however, the technology used allows good control of the fixture of these bridges as illustrate in Fig. 2.

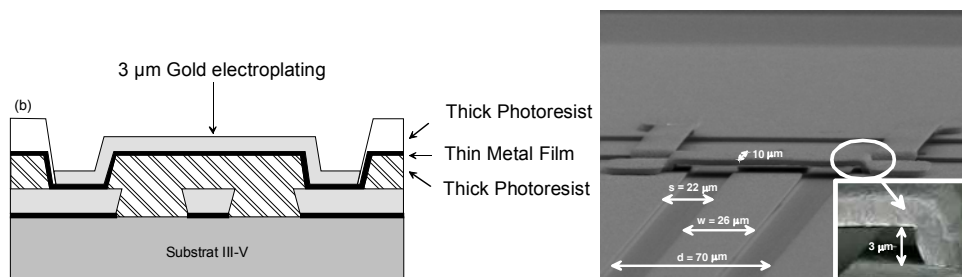


Fig. 2. Air-bridge realization: (a)- Lithography process, (b)- Airbridges realized with IEMN technological process.

In order to minimize the parasitic influence of the bridge on the electrical characteristic of the lines and provide mechanical stability, the dimensions of the air bridge used are: 3  $\mu\text{m}$  height, 10  $\mu\text{m}$  width, 80  $\mu\text{m}$  length ( $d=70 \mu\text{m} + 10 \mu\text{m}$  minimum spacing between slot border and bridge), and 3- $\mu\text{m}$  metal thickness. Moreover, to give it a good mechanical stability, a maximum length must be defined for a given width: for example, 10  $\mu\text{m}$  and 20  $\mu\text{m}$  widths allow maximum lengths of 100 and 180  $\mu\text{m}$ , respectively. Although the bridge introduces an excess capacitance, this does not constitute a problem for the bridge widths here as long as the strip widths of the coplanar line are all kept small. Under a configuration with these dimensions, no compensation techniques, such as using sections of high-impedance line, are required (Rius et al., 2000-a), (Weller et al., 1999).

## 2.2 Optimal dimensions for coplanar transmission lines

So as to determine the optimum sizing of coplanar transmission lines, we rely on the work of W. Heinrich (Heinrich, 1993). The proposed quasi-TEM description ensued from a quasi-static approach. The *RLCG* equivalent circuit components are determined from approximate analytical equations derived from a global analysis. These values depend for electrical and geometrical parameter of the transmission lines as well as the frequency. *C* and *G* elements are considered invariant with frequency. However, as the skin effect modifies the current distribution in conductors depending on frequency, the *R* and *L* elements are highly dependant on frequency. For instance, let us consider a 50  $\Omega$  coplanar transmission line implemented in GaAs technology ( $h=400 \mu\text{m}$ ,  $t=3 \mu\text{m}$ ,  $\epsilon_r=11.9$ ,  $\tan\delta=2\times 10^{-4}$ ,  $\sigma=4.1\times 10^7 \text{ S.m}$ ) with line- and slot-width of  $W=26 \mu\text{m}$ ,  $S=22\mu\text{m}$ , respectively. Fig. 3 illustrates the evolution of the *R* and *L* parameter for transmission line model as a function of the frequency.

With knowledge of *RLCG* parameters, one can easily determine the parameters of propagation, attenuation, impedance and effective permittivity and, therefore optimal rules for transmission line sizing as a function of its geometrical parameters: line- and slot-widths as well as ground-to-ground distance. The inter-ground distance ( $d=W+2 \cdot S$ ) is an important parameter for wave propagation. Indeed, so as to avoid propagation of parasitic modes, this distance  $d$  has to be low compared to the wavelength; the commonly used constraint is  $d \leq \lambda_g/10$ . An increase of this constraint ( $d \leq \lambda_g/20 = d_{max}$ ) allows neglecting the radiation losses. Moreover, it limits extend of radiating waves, and therefore the problems relied to packaging. However, according to Fig. 4-(a), the attenuation also depends on the ground-to-ground distance. It is, in fact, inversely proportional to the distance  $d$ . It follows that inter-ground distance  $d$  must be the closest to  $d_{max}$ .

Once the inter-ground distance chosen, we are interested in the relation between the dimensions of the line-width and inter-ground distance. This ration  $W/d$  is predominant in the choice of the achievable characteristic impedances. According to Fig. 4-(b) so as to limit the attenuation, it is preferable to set  $W$  in the interval between  $0.3 \times d$  and  $0.6 \times d$ . Moreover, the ground plane width ( $W_g$ ) and the substrate thickness ( $h_s$ ) are chosen to make a trade-off between losses and low dispersion up to the W-frequency band. To summarize, the following conditions are then chosen to realize our devices:

$$d = (W + 2 \cdot S) \leq \frac{\lambda_g}{20} = d_{max} \quad (1)$$

$$0.3 \cdot d \leq W \leq 0.6 \cdot d \quad (2)$$

$$W_g \geq W + 2 \cdot S \quad (3)$$

$$h_s \geq 2 \cdot (W + 2 \cdot S) \quad (4)$$

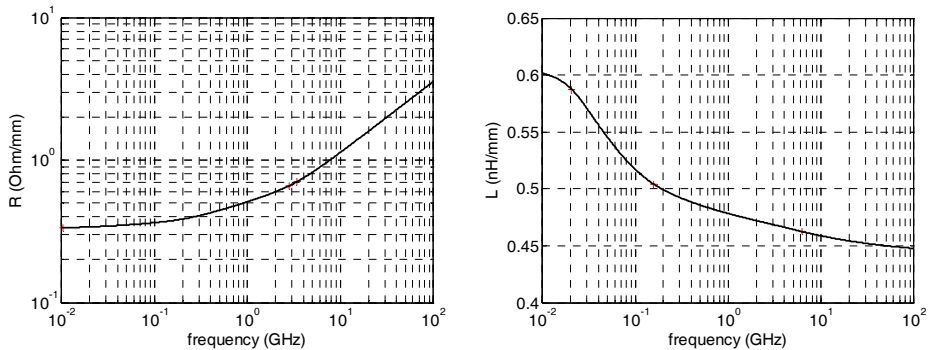


Fig. 3. Evolution of  $R$  and  $L$  parameters as a function of the frequency.

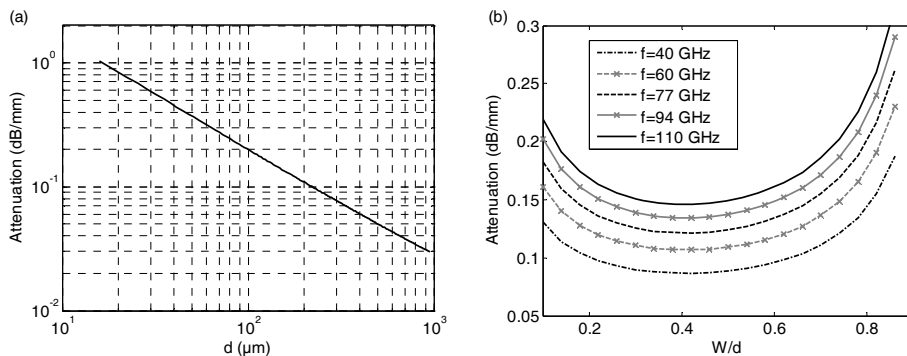


Fig. 4. Evolution of the attenuation as a function of : (a) ground-to-ground distance. (b) Line width ( $W$ ) to ground-to-ground ( $d$ ) ration.

### 2.3 Wide-band bandpass filter design

We first investigated on the design of quarter-wavelength shunt-stub filters. Such topology includes shorted stubs as resonators separated by quarter-wavelength transmission lines as inverters. The synthesis developed by Matthaei (Matthaei et al., 1980) indicates that the bandwidth is in close relation with the impedance level of the resonators. In the present case, so as to respect optimal sizing described above the impedance range extends from  $30 \Omega$  to  $70 \Omega$ . Thus, the available 3-dB bandwidth will be approximately bounded by 100% and 36%. For bandwidths below 36%, very low impedance levels are needed. Thus, shape factors become too large for correct performance from the device with regard to both the parasitic influences of the discontinuities and modelling difficulties. So, other topologies such as coupled-line filters are preferred.

The first results presented here deal with 58% and 36%, 3-dB-bandwidth, 3<sup>rd</sup>-order filters centred on 82.7 GHz. According to synthesis, the first example with 58% 3-dB-bandwidth results in a  $25 \Omega$  impedance for the resonators when inverters are kept to  $51 \Omega$ . Twenty-five is chosen so as to introduce double  $50 \Omega$  stubs for the resonator (Fig. 5-(a)). According to the low level of insertion losses, the standard geometry was chosen as follows:  $26 \mu\text{m}$  for the strip widths and  $22 \mu\text{m}$  for the slot widths. The 36% bandwidth was reached by selecting impedances of  $56 \Omega$  and  $15 \Omega$  for inverters and resonators, respectively. As before,  $15 \Omega$  was obtained with two double  $30 \Omega$  stubs. It corresponds to the lowest bandwidth that can be reached with an impedance range bounded by  $30 \Omega$  and  $70 \Omega$ . For the inverters, strips and slots were  $20 \mu\text{m}$  and  $25 \mu\text{m}$ , respectively, and  $54 \mu\text{m}$  and  $8 \mu\text{m}$  for the resonators. The layout and frequency response are displayed in Fig. 5-(b). As for the first prototype, experimental and simulated results agree over a broad-band frequency.



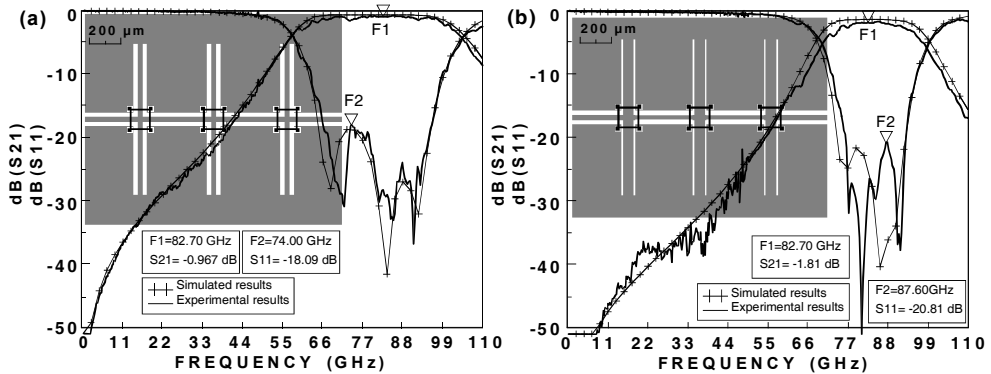


Fig. 5. Layout, simulated, and experimental associated magnitude responses of the 82.7-GHz central-frequency, (a) 58% 3-dB-bandwidth and (b) 36% 3-dB-bandwidth filters.

As shown in Fig. 5, insertion losses increase with filter selectivity: 0.96, and 1.81 dB are obtained for 58%, and 36% bandwidth filters, respectively. These values are in complete agreement with the following expression (Matthaei et al., 1980), (Cohn, 1959):

$$I.L. = \frac{4.343 \cdot n}{Q_u \cdot w} \tag{5}$$

with *I.L.* the insertion loss in decibels, *n* the filter order, *w* its relative bandwidth, and *Q<sub>u</sub>* the unloaded quality factor, which is close to 25 for the standard 50 Ω transmission line used here.

### 2.5 Narrow-band bandpass filter design

Two major problems are related to narrow-band bandpass coupled-lines filters. First, insertion losses become important when the selectivity of the filter is increased. The second problem deals with accuracy which is directly in relation to the level of selectivity.

In order to illustrate this, we present the results obtained with two classical coupled-lines third-order bandpass filters. The first one is at a center frequency of 65 GHz, 22% 3-dB bandwidth whereas the second one is at 94 GHz, 5% 3-dB bandwidth. Figs. 6 and 7 show the layouts of these filters. For such topologies, according to well-known synthesis (Matthaei et al., 1980), the bandwidth and the coupling coefficient level of the coupled-lines sections are in close relation. Indeed, narrow selective bandwidths are obtained with low coupling levels on the central sections of the filter. A convenient solution consists of using a separating ground plane between the coupled strips. This leads to low coupling levels on a reduced bulk and this separate ground plane acts as a good parasitic mode filter (Fig. 7). According to the finite conductivity of the metal ( $4.1 \times 10^7$  S.m for gold metallization) and to the dissipation factor of the GaAs substrate ( $\tan\delta=2 \times 10^{-4}$ ), very high insertion losses are expected when designing such narrow-band filters. These insertion losses can be predicted roughly from (5). For instance, for a third-order, 22% 3-dB-bandwidth coupled-line filter designed with 26-μm strip widths, insertion losses between 1.95 dB and 2.95 dB are obtained. However, if the bandwidth is decreased to 5%, insertion losses reach a critical



level between 8.7 and 13 dB. These values were calculated with the unloaded quality factor of 20 and 30. One way of improving this critical point is to increase the strip widths, but this gives rise to several problems. The first problem concerns the bridge topology: a large ground-to-ground spacing is, indeed, forbidden because of mechanical stability constraints. A good way to solve this problem is to fabricate an inter-strip bridge as shown in Figs. 6 and 7. By doing so, the ground connections used for filtering the coupled-slotline modes are made directly with a tiny strip on the first metallization layer.

The second one concerns modelling. Obviously, as the strips are wider, the conditions of low dispersion given in Section 2.2 are not necessarily still valid. Moreover, the validity conditions of the analytical quasi-TEM models used are not always met. Finally, the dimensions of the discontinuities increase with the strip widths and, consequently, strong parasitic effects appear. Modelling them accurately is quite difficult and it allows only an approximation. Nevertheless, as an optimization procedure is needed to adjust all the characteristics of the filter response correctly, it requires the use of a very fast modelling technique (Prigent, et al., 2004-b). As shown in Fig. 6 for the 22% 3-dB-bandwidth prototype a good agreement is observed between simulated and experimental results. This agreement is valid over a wide frequency band from 500 MHz to 110 GHz and, as expected, correct insertion loss levels of about 1.4 dB are observed in the bandwidth.

Since the bandwidth is very selective, the measurements were only made on a frequency range from 66 to 110 GHz for the second prototype. The experimental results are presented in Fig. 7 and give a 4-dB insertion loss and 10-dB return loss for a centre frequency of 91.5 GHz. Compared to the expected results, one should also note a significant bandwidth broadening. In this case, this problem is only due to the reverse side of the substrate. Indeed, as the ground-to-ground spacing is very large, the electromagnetic fields are strongly modified by the electrical condition on the reverse side of the dielectric substrate: open or grounded. Impedance and coupling levels are subject to changes that significantly modify the frequency response. Post-simulation was carried out to check the bandwidth broadening by taking into account correct conditions on the substrate backside. This post-simulation is presented in Fig. 7. As this problem masks the errors due to the modelling method, it is difficult to form any conclusions regarding its accuracy in this frequency range. Although the insertion loss appears to be correct, new experiments on filters with a correct bandwidth and return loss are necessary to assess the insertion loss accurately. Nevertheless, when designing future very high-selectivity filters for which the confinement of the electromagnetic field is a problem, the designer must keep in mind the packaging aspect. As grounded CPW lines are not a very convenient solution, three-dimensional technological solutions using, for instance, thin- or thick-film microstrip transmission lines appear to be equally well suited (Rius et al., 2000-b), (Six et al., 2001), (Aftanasar et al., 2001), (Warns et al., 1998), (Schneider & Heinrich, 2001).

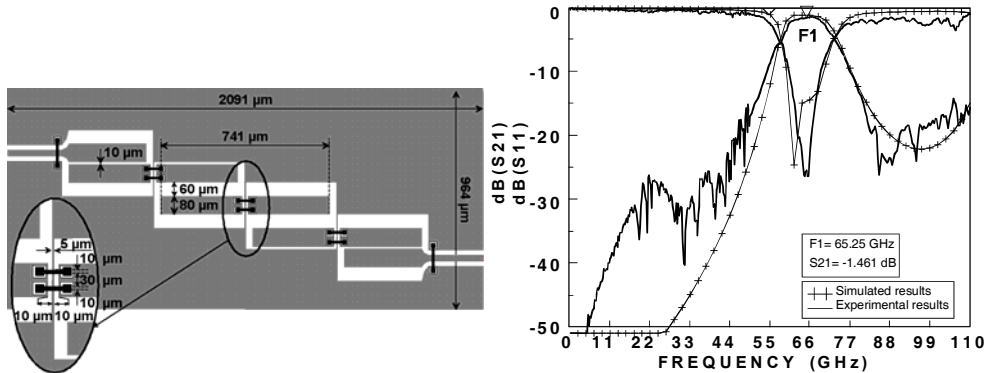


Fig. 6. Layout, Simulated and experimental results of a 65-GHz central-frequency, 22% 3-dB-bandwidth, coupled-line filter.

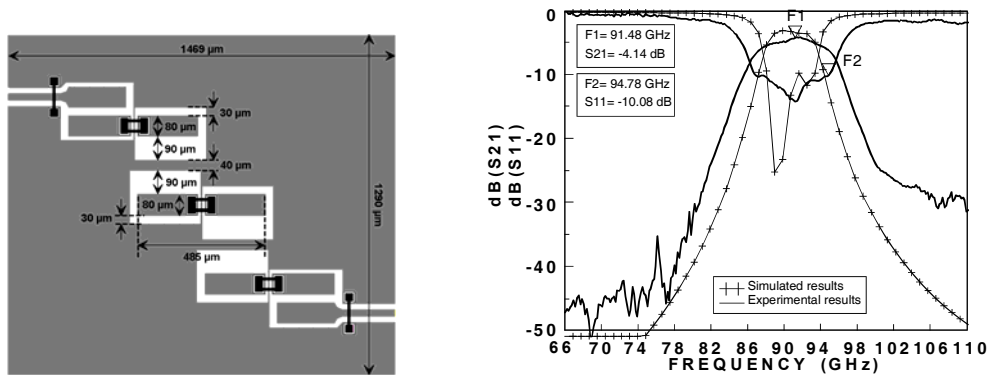


Fig. 7. Layout, Simulated and experimental results of a 65-GHz central-frequency, 5% 3-dB-bandwidth, coupled-line filter.

### 3. Membrane Technologies

#### 3.1 Technological process

Contrary to the previously described III-V technologies which production cost limits their use to little series, technologies on silicon offer an interest with respect to cost reduction while retaining their interest in the integration of active functions. Nevertheless their major drawback is that levels of dielectric losses are not compatible with the specifications required for the passive functions. An alternative consists in the use of silicon membrane technology whose primary function is to mechanically support circuits while remaining transparent for functions in microwave. Thus, the electrical characteristics of this support match with those of vacuum, the ideal dielectric. On the other hand, membrane technology permits to minimize phenomena of dispersion, as well as the removal of cavity modes.

The technological process developed here is nearly the same as the one developed in III-V technology. The major difference is the membrane realization and the backside etching of the silicon. The membrane technology developed at the LAAS laboratory (Toulouse, France)

is realized on a 400- $\mu\text{m}$ -thick silicon substrate ( $\epsilon_r = 11.9$ ,  $\tan\delta = 0.018$ ). The technological process is composed of five main steps as depicted in Fig. 8.

The first step consists in a deposition of two layers  $\text{SiO}_2$  (0.8  $\mu\text{m}$ ,  $\epsilon_r = 4$ ) and  $\text{Si}_{3.4}\text{N}_4$  (0.6  $\mu\text{m}$ ,  $\epsilon_r = 8$ ) realized on both size of silicon wafer. Then,  $\text{SiO}_{0.7}\text{N}_{0.7}$  layer (5  $\mu\text{m}$ ,  $\epsilon_r = 5.5$ ) is deposited on the front side. Next, the elaboration of metal level is performed by first the evaporation of a Ti/Au seed layer and then a 3  $\mu\text{m}$  gold electroplating into a photoresist mould. After the suppression of photoresist mould, the seed layer is suppressed in the slots. The third step is to realize air bridges. A photoresist mould is used to fill up coplanar slots. A sacrificial layer with the same type of photoresist mould is then deposited to form air bridges. A gold seed layer is evaporated and then 3- $\mu\text{m}$ -thick gold is electroplated. The plating is followed by gold etching. The next step consists in realisation membrane by removing silicon substrate in the back side. Silicon etching is realized by dry way using Deep Reactive Ion Etching (DRIE) technique through a thick photoresist mould. Moreover, to protect air bridges and to avoid the membrane breaking during DRIE process, the wafer is bonded to a support one in the front side. Finally, the structures are released from the support substrate using acetone bath followed by  $\text{CO}_2$  drying process. With these three layers of dielectric, the membrane possesses a mechanical stiffness strong enough to absorb the stresses induced by various technological processes while retaining effective permittivity of 1.8 which is close to 1.

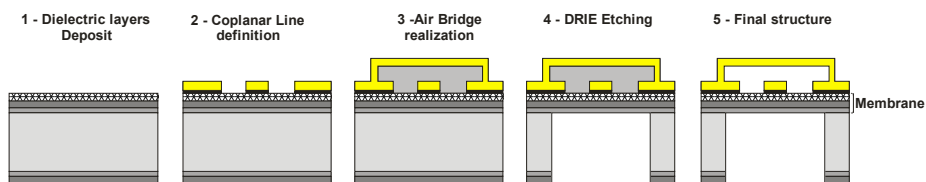


Fig. 8. Membrane technological process

### 3.2 Wide-band bandpass filter Design

The use of such technology has already been the subject of many studies and has demonstrated its effectiveness for circuits in millimetre band and for low frequencies operating (C-band). Nevertheless, its use in W-band is reported to be more sensitive concerning the required level of technological accuracy. While membrane technologies offer an interest in the reduction of dielectric losses, a permittivity close to 1 severely limits their use in terms of achievable impedances. Indeed, when meeting the conditions described by Heinrich (Section 2.2) so as to limit both the dispersion of the transmission lines and losses, for a relative permittivity of 1.8, the ground-to-ground dimension ( $d$ ) is about 230  $\mu\text{m}$  @ 94 GHz. Within these conditions, the strip width should be set in an interval between 65  $\mu\text{m}$  and 140  $\mu\text{m}$ , which makes the achievement of 50  $\Omega$  transmission line impossible. However, as the membrane technology is less dispersive than the III-V technology, the constraints can be relaxed to release limits in the impedance range. Thereby,  $W$  was chosen to be in an interval between 33  $\mu\text{m}$  and 199  $\mu\text{m}$ , this lead to achievable characteristic impedances from 50  $\Omega$  to 138  $\Omega$  at 94 GHz.

The filter presented here a classical 4<sup>th</sup>-order shunt-stubs filter with centre frequency of 94 GHz. Despite the degree of freedom is available in the synthesis (Matthaei et al., 1980) which permits to adjust impedance values, the limitation of the achievable impedance range for

membrane technologies does not allow us to reach bandwidth less than 55%. Nevertheless, the use of topology with dual stubs allows us to achieve narrower bandwidth. The layout of a 4<sup>th</sup>-order filter with dual short-ended stubs at 94 GHz is displayed in Fig. 9-(a). An insertion loss of 2 dB for a relative bandwidth of 45% is obtained by electromagnetic simulation HFSS (Fig. 9-(b)). Experimental results were made from 60 GHz to 110 GHz.

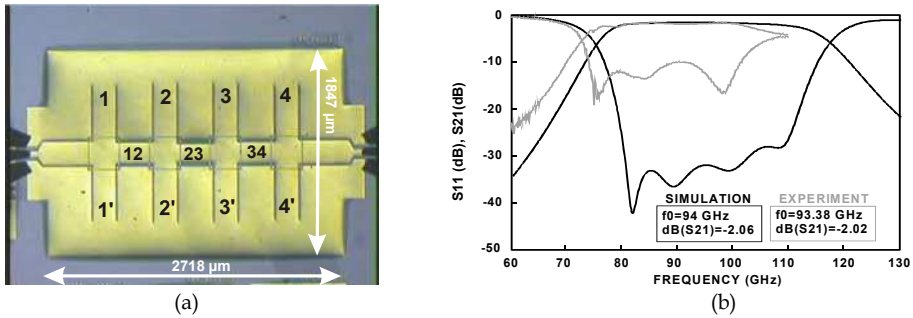


Fig. 9. 4<sup>th</sup>-ordre classical shunt-stubs bandpass filter. Photograph (a), Simulated and experimental magnitude responses (b)

Based on the previous filter topology, we have developed a 4<sup>th</sup>-order filter with folded stubs in short-circuit termination. The benefit of such a structure is to promote a coupling between non-adjacent resonators. Thus, it creates a transmission zero whose frequency depends on the nature of the coupling created. For electrical coupling (capacitive) it creates a zero in a high frequency, while magnetic coupling (inductive) will create a zero in a low frequency. In the case of study, stubs were in short-ended termination, so we promoted a generation of magnetic coupling between stubs 1'-3 and 2'-4 (Fig. 10-(a)). The response of such a filter (Fig. 10-(b)) has a bandwidth of 37.6% and an insertion loss of 1.685 dB. An apparent reduction in the band is due to the presence of a transmission zero at low frequency. Thus, it is possible to relax constraints on the nominal filter bandwidth consequently resulting in a slightly reduced insertion loss. In comparison with experimental results, we can notice that there is a 4 GHz frequency shift. In regards to the complexity of such a topology, the results are however satisfactory.

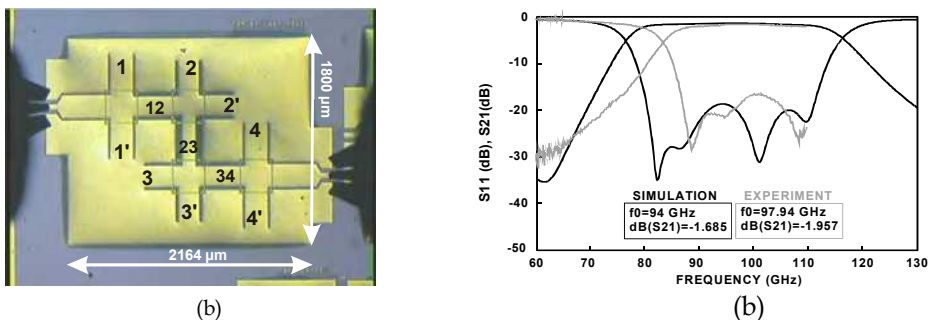


Fig. 10. Filter with folded stubs. Photograph (a), Simulated and experimental magnitude responses (b)

### 3.3 Narrow-band bandpass filter Design

The proposed technology has proven to be appropriate for achieving broadband filters. However, the difficulties met in the design of bandpass filters are tougher for achieving a filter with narrow bandwidth (5% 3-dB bandwidth). With the use of classical coupled-line filters, when designing a filter at 94 GHz we are facing technological impossibilities. Technological constraints impose line- and slot-widths to be greater than  $10\ \mu\text{m}$ . Inter-ground distances of coupled lines are large, which yields a difficulty to ensure the continuity of ground, and on the other hand, problems of mechanical stability of inter-ground bridges. Moreover, in considering the low permittivity and electrical lengths at 94 GHz, we are faced with coupled lines whose width to length ratio is too large (Vu et al., 2008). Therefore, the topology we developed is a pseudo-elliptic filter with ring resonator. Such a filter is characterized by the presence of two separate propagating modes, which create transmission zeros. The separation of the two modes of propagation is usually ensured by the introduction of discontinuities in the ring. In our case we used a topology with lateral coupled-lines access which synthesis was developed by M.K. Mohd Salleh (Mohd Salleh et al., 2008). This 2<sup>nd</sup>-order ring-based filter at 94 GHz has a relative bandwidth of 5%. It consists of two quarter wavelength lines excited by two identical quarter wavelength coupled-lines. The joint use of such a simplified topology and synthesis made the design ease and strongly limited the tuning steps. The electromagnetic simulations (Fig. 11) show a 5.3% bandwidth for an insertion loss of 3.57 dB and a return loss of 19 dB at 94 GHz. Experimental and simulated results are in good agreement. An insertion loss of 6.46 dB at 94.69 GHz and a return loss better than 20 dB are obtained for experimental results.

However, despite quite good results for the proposed filter, the membrane technology suffer form major drawbacks that limit its use for the filter design: the first one concerns the limited achievable impedance range; the second concerns the low permittivity which, while interesting to limit the dispersion of the line, limits its use to relatively low frequency range; the last one concerns technological aspect, since Silicon etching shape which is realized by dry way using Deep Reactive Ion Etching is difficult to control. Therefore, one has to develop new technologies to implement passive functions in millimeter frequency range.

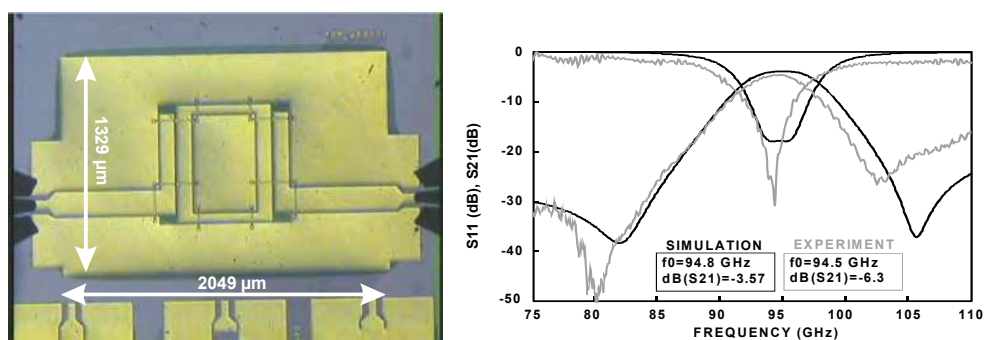


Fig. 11. 2<sup>nd</sup>-order ring resonator filter. (a) Photograph. (b) Simulated and experimental results.

## 4. Thin Film Microstrip (TFMS) Technologies

### 4.1 Technological process

The TFMS technology presented hereafter can be either implemented on III-V or silicon substrate. However, it is particularly well suited for silicon based technology. Indeed, benefits of silicon technology are undisputable in the design of active devices. Nevertheless, according to the silicon low resistivity ( $\rho \approx 10 \Omega \cdot \text{cm}$ ), implementation of passive devices is difficult because of the high insertion-loss levels. As our purpose was to keep the silicon substrate for implementation of active functions, an alternative consisted in the use of silicon as mother board. Passive functions are then transferred to a dielectric layer [Benzocyclobutene (BCB)] deposited on the motherboard, the dielectric layer and silicon being insulated via a ground plane. The presence of this ground plane allows avoiding dielectric-loss effects related to the silicon low-resistivity. Moreover, well-supplied libraries with various models are available for such a technology, microstrip by nature.

The first step of the technological process (Fig. 12.) is ground plane achievement through the deposition of a 3- $\mu\text{m}$ -thick layer of electroplated gold. So as to ensure the metal growth, thin-tungsten and gold-based adhesion films (200 Å/ 300 Å) were first deposited by evaporation. Due to poor adhesion between BCB and gold, a 300-Å-thin film of titanium was evaporated on the ground plane.

The dielectric we used was the photosensitive BCB 4026-26 from Dow Chemical, Midland, MI, ( $\epsilon_r=2.65$ ,  $\tan\delta=2.10^{-3}$ ). It allows a 10- $\mu\text{m}$ -thick layer deposition. The first photosensitive BCB film was then spin coated onto the Ti film. The BCB film thickness is a function of subsequent processing steps, including pre-baked conditions, spin coating speed, exposure dose and development. After these processing operations, BCB pads of 10  $\mu\text{m}$  thickness were obtained. A soft baking (up to 210° C) of this first dielectric was made to ensure resistance to subsequent processing operations. The second 10- $\mu\text{m}$ -thick BCB film polymer film was then spin coated and patterned (photolithography: UV light exposure and DS2100 developer) in the same way as the first layer. Then a final hard baking for polymerization was performed from in-stage annealing up to 230 °C. The signal transmission lines as well as the coplanar accesses were fabricated at the same time. The coplanar accesses on the top of BCB were connected to the ground plane through the sides of the dielectric. In order to obtain metallization using gold electroplating, a bi-layer photoresist was used. The first photoresist layer is used to protect other devices. After the spin coating of the photoresist and the photolithography process (pre-baking, exposure and development), transmission lines and coplanar accesses with wider dimensions (3  $\mu\text{m}$ ) were made. A thin conductor film (Ti/Au, 300 Å/200 Å) for electroplating was then evaporated, and the second thick photoresist layer (greater than the envisaged metallization thickness) is spin coated and photoprocessed to define the exact dimensions of the transmission line and coplanar access. After electroplating of 3  $\mu\text{m}$  of gold, the upper photoresist was removed using a photoresist developer stage. The thin conductor film was removed with wet-etching, and the lower photoresist was finally diluted with a remover. The transmission line structure obtained is illustrated in Fig. 13.

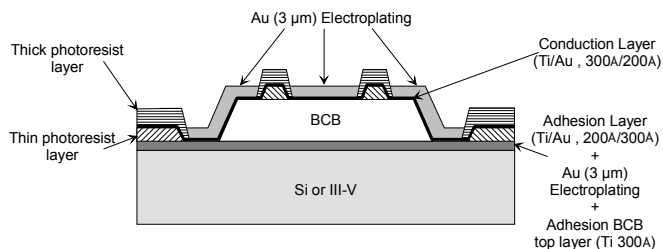


Fig. 12. Technological process for BCB-based transmission line.

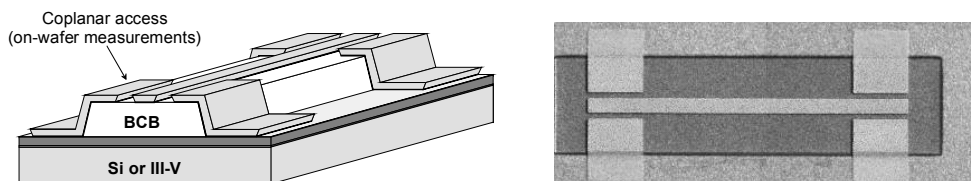


Fig. 13. Topology and microphotograph of a 50- $\Omega$  transmission line in TFMS.

Previous works have shown that the BCB layer thickness is a parameter that most influences the losses (Six et al., 2005), (Leung et al., 2002), (Prigent et al., 2004-a). Investigations were carried out so as to reduce these insertion losses. As shown in Fig. 14, the transmission line attenuation decreases with the BCB thickness increase. It was shown that a 20- $\mu\text{m}$ -thick BCB layer can be considered as the optimum dielectric thickness. Beyond 20- $\mu\text{m}$ -thick, no significant attenuation improvement was obtained. Within such a topology, measurements were performed through a broad frequency range from 0.5 GHz to 220 GHz.

Transmission line with 50- $\Omega$  impedance was calibrated out. This was achieved by means of thru-reflection line calibration method (TRL). The calibration standards and transmission line were fabricated on the same wafer. HP 8510 XF and Anritsu 37147C network analyzers were used in the (45 MHz-120 GHz) and (140 GHz-220 GHz) frequency range, respectively. Simulated results and experiments are in a good agreement in a wide frequency range. Attenuation measured for a 50- $\Omega$  transmission line at 220 GHz is of the order of 0.6 dB/mm (Fig. 15).

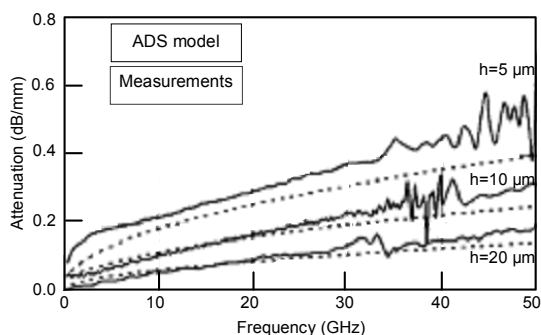


Fig. 14. Attenuation of 50- $\Omega$  TFMS-lines for different BCB thickness. Comparison between simulation and experimental results



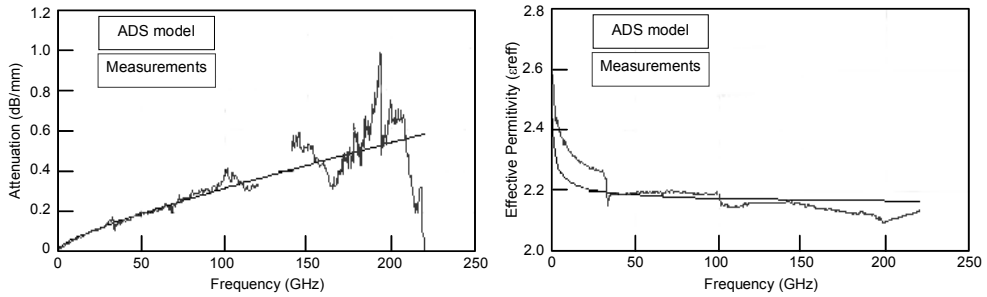


Fig. 15. Comparison between simulation (ADS) and measurement results of a 50- $\Omega$  TFMS-line with 20- $\mu\text{m}$  BCB thickness up to 220 GHz.

#### 4.2 Bandpass filter Design

So as to illustrate the Si-BCB based thin film microstrip technology, the filter to be designed roughly corresponds to a U-band filter, the 3-dB passband is 49–51 GHz, the rejection level in the 41.15–46.15-GHz frequency band is 35 dB, and no specification for the upper band beyond 51 GHz is required.

Coupled-line topologies are basically well suited for narrow bandpass filters. Nevertheless, in view of the desired insertion losses and rejection levels, such topologies become unsuitable with the above filter specifications. Indeed, the closeness of the passband and lower reject band imposes high rejection levels. Hence, the filter order has to be increased, which significantly degrades global insertion losses. These considerations have led us to choose a new filter topology based on dual behavior resonators (DBRs), which means both stopband and passband (Rizzi, 1988). Such a resonator results from two different open-ended stubs set in parallel. Each stub brings a transmission zero on either side of the passband. Development of a global synthesis enabled us to independently control the bandwidth, the upper and lower frequency bands, as well as the different transmission-zero frequencies of an  $n^{\text{th}}$ -order filter, *i.e.*, composed of DBRs (Quendo et al., 2003). Let us apply an alike development to the design of a 4<sup>th</sup>-order filter that meets the desired specifications. It results in a filter with four transmission zeros on both sides of the passband. These transmission zeros being independent, their frequencies are either separated or joined. This depends on the electrical length of the four resonators: they can differ or be identical (Fig. 16). For the sake of simplicity, the electrical characteristics of the upper frequency stubs, *i.e.*, (L1a, Z1a), (L2a, Z2a), (L3a, Z3a) and (L4a, Z4a), were chosen equal, which meant that the upper transmission zeros were joined. Similarly, the lower frequency stubs were of equal length, *i.e.*, (L1b, L2b, L3b, and L4b), and the associated transmission zeros were joined. The filter was designed based on the joint use of the synthesis (Quendo et al., 2003) and the DOE based design method that allows simple and rapid correction process (Prigent et al., 2003-a), (Prigent et al., 2003-b), (Tagushi, 1987), (Prigent et al., 2002). As depicted in Fig. 17, the filter electrical response obtained with this design method was in a very good agreement with the simulations results (ADS-Momentum).

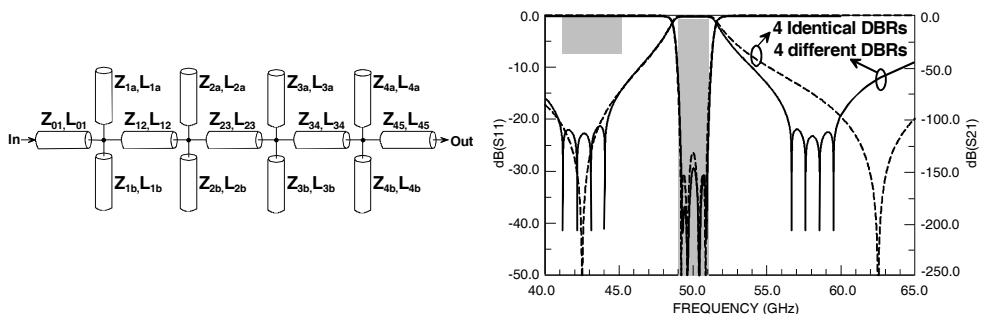


Fig. 16. 4<sup>th</sup>-order ideal DBR topology and response : with different resonator type (impedance and length) or with four identical resonators.

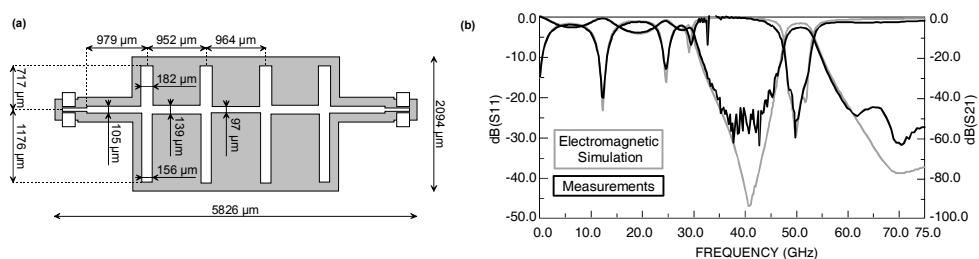


Fig. 17. (a)Layout of the 4<sup>th</sup>-order DBR filter in U-band. (b) comparison of electromagnetic simulation with experiment, in wide frequency range up to 75 GHz (c).

### 4.3 Application in the G-band (140 GHz-220 GHz)

According to the quality of the experimental results observed at 94 GHz, one has attempted to transpose our concepts to upper frequency domain in G-band (140-220 GHz). In this frequency range, the problems due to sensitivity and design accuracy are all the more important since the electrical lengths that are involved are very small.

Let us consider the design of a 4<sup>th</sup>-order classical shunt-stubs filter with 10% 3-dB-bandwidth. According to classical synthesis (Matthaei et al., 1980), while designing filter with such specifications, we are faced to technical impossibilities. Indeed, at this frequency level, transmission lines are wider than long. Hence, the electromagnetic simulation results are strongly debased. Moreover, the filter dimensions made the electrical response correction difficult, indeed impossible. So as to overcome such a difficulty, the solution we have developed (Prigent et al., 2005) consists in considering the first harmonic as the frequency of interest, not the fundamental frequency. Thus, the filter to be designed is a 4<sup>th</sup>-order filter with 60 GHz central frequency. In this way, one can reach the filter specifications while keeping a correct shape factor for the stubs (Fig. 18). Measurement results were made in 0-110 GHz and 140-220 GHz bands. Despite a slight insertion losses improvement, the measurement results are in a complete accordance with the desired specifications.

## Thank You for previewing this eBook

You can read the full version of this eBook in different formats:

- HTML (Free /Available to everyone)
- PDF / TXT (Available to V.I.P. members. Free Standard members can access up to 5 PDF/TXT eBooks per month each month)
- Epub & Mobipocket (Exclusive to V.I.P. members)

To download this full book, simply select the format you desire below

